SLAC-TN-07-010
August 2007

Measuring Strain Using X-Ray Diffraction

James Belasco

Office of Science, SULI Program

Villanova University

Stanford Linear Accelerator Center

Menlo Park, CA

August 17, 2007

Prepared in partial fulfillment of the requirements of the Office of Science, U.S. Department of Energy Science Undergraduate Laboratory Internship (SULI) Program under the direction of Dr. Michael Woods at the Stanford Linear Accelerator Center.

Participant: _____
Signature

Research Advisor: _____
Signature

Work supported in part by US Department of Energy contract DE-AC02-76SF00515

Table of Contents

Abstract

Measuring Strain Using X-Ray Diffraction. JAMES BELASCO (Villanova University, Villanova, PA, 19085) APURVA MEHTA (Stanford Linear Accelerator Center, Menlo Park, CA, 94025)

Determining the strain in a material has often been a crucial component in determining the mechanical behavior and integrity of a structural component. While continuum mechanics provides a foundation for dealing with strain on the bulk scale, how a material responds to strain at the very local level—the understanding of which is fundamental to the development of a cohesive framework for the behavior of strained material—is still not well understood. One of the critical components in determination of the behavior of materials under strain at a local scale is an understanding how global average deformation, as a response to an externally applied load, gets distributed locally. This is critical and very poorly understood for a polycrystalline materials—the material of choice for a large variety of structural components. We studied this problem for BCC iron using x-ray diffraction. By using a nanocrystalline iron sample and taking x-ray diffraction patterns at different load levels and at different rotation angles, a complete 2^{nd} rank strain tensor was determined for the three sets of crystallites with three distinct crystallographic orientations. The determination of the strain tensors subsequently allowed the calculation of the elastic modulus along each crystallographic plane. When compared to measured values from single crystal for the corresponding crystal orientations, the data from our polycrystalline sample demonstrated a higher degree of correlation to the single crystal data than expected. The crystallographic planes demonstrated a high degree of anisotropy, and therefore, to maintain displacement continuity, there must be a secondary mode of strain accommodation in a regime that is conventionally thought to be purely elastic.

Introduction

Every successful major bridge builder for half a century has used continuum mechanics to analyze the response of materials to strain. However, while continuum mechanics can model the deformation of materials at large scales, at the very local scale materials invariably deform and fail, (even in large structures failure is often initiated by a single crack). At the very local scale, materials are not the homogeneous and isotropic structures continuum mechanics assumes them to be, but instead are composed of an anisotropic arrangement of discreet atoms and molecules. Thus, a more complete understanding of mechanical behavior is necessary to reconcile the discrepancy between the two views of the behavior of materials as they are subjected to stress.

The two types of strain, classified as plastic, or irreversible strain, and elastic, or reversible strain, produce two different types of perturbations in the lattice structure of a material. Elastic strain causes a stretching in the lattice bonds while plastic strain results in dislocation and motion of slip-bands. The ideal method for measuring such changes is X-ray diffraction, which produces a distinctly different pattern for the two different types of strains. Elastic strain, which is the primary focus of this paper, alters the spacing of the crystalline lattice and therefore results in shifting of the diffraction peaks [2]. Thus, as a sample is strained along a particular axis, X-ray diffraction patterns can be taken that will elucidate the deformation in the lattice structure. Using BCC iron, a ring pattern can be obtained that can be mathematically analyzed to generate the full second order strain tensor. These tensors thereby indicate the particular deformation of the sample under strain as it responds along multiple axes. By calculating the strain tensors for each of the three diffraction rings of iron, the (110), (200), and (211), (each of which corresponds to

a different crystallographic orientation) and comparing them to one another the deformation of the crystallites with those crystallographic orientations can be determined. Ultimately, the elastic modulus of each lattice plane can be calculated through an analysis of the change in the strain level for increasing load levels.

Materials and Methods

Sample Preparation

BCC iron samples with a thickness of 13.5 microns were prepared for x-ray diffraction by cutting them into dog bone shapes that were then inserted into a displacement controlled tensile rig. The dog bone shape is used to facilitate purely tensile loading and limit the amount of out of plane strain in the material

Data collection Procedure

X-ray diffraction patterns (see Figure 1) were taken with a set wavelength of 0.975 Å as the prepared iron samples were rotated from 0 degrees to + 45 degrees with a diffraction pattern taken every 9 degrees. To study the elastic deformation, the sample was strained to the onset of plastic deformation (the plastic strain limit taken to be that determined by traditional continuum mechanics sources) and the diffraction patterns were taken at set intervals as the sample was unloaded, to ensure that at least under conventional mechanics model the subsequent deformation is purely elastic. Patterns were taken at five separate load levels as well as at the initial zero load level.

Pattern Analysis

An unstrained lattice produces a diffraction pattern with circular rings. When a sample is under elastic tensile stress, the lattice spacing elongates in the direction of the applied load and contracts in the orthogonal directions. This results in an elliptical

distortion of the diffraction rings. The eccentricity of these ellipses directly corresponds to how the sample has deformed under strain. In order to analyze the nature of this ellipse, the 2-D diffraction images were converted to diffraction coordinates (Q, chi) from pixel positions using Fit2D. Fit2D itself was calibrated for specific measurements using LaB_6 samples that have standardized diffraction parameters. The eccentricity of the ellipse and the resulting magnitude of all the six independent components of the 2nd rank strain tensor were determined from this converted data by the procedure outlined below.

Strain Tensor Determination

The change in ellipticity of a diffraction ring under load is seen as a noticeable fluctuation (termed "wiggle") in the normally straight line of the Q vs. chi polar plot (see Figure 2). Using a program developed in MATLAB®, a Gaussian fit was used to determine the location of the high intensity points of the wiggle (Figure 3), the magnitude of the intensity, and the width of the intensity curve. The resulting Q and chi coordinates of the intensity peaks were then transformed into the psi and phi coordinates used in the standard $\sin^2\Psi$ technique [1]. These calculated values were then used to generate the coefficients for the strain tensors equation according to:

$$\varepsilon_{\Phi} = \varepsilon_{11}\cos^2\Phi\sin^2\psi + \varepsilon_{22}\sin^2\Phi\sin^2\psi + \varepsilon_{33}\cos^2\psi + \varepsilon_{12}\sin 2\Phi\sin^2\psi + \varepsilon_{23}\sin\Phi\sin 2\psi + \varepsilon_{13}\cos\Phi\sin 2\psi \quad (1)$$

Where: $\varepsilon_{\Phi\psi} = \dfrac{d_{\Phi\psi} - d_0}{d_0}$ (2)

And the change in d is the displacement of the sample as it stretches under strain. For each load level, the MATLAB® program takes data from all the diffraction patterns as output by Fit2D and then uses the collective data points from each strain level in a least-squares fit, weighted by widths provided by the intensity curves, to solve for the second

order strain tensors (ε_{ij}) as well as generate the error values for each calculated tensor. This process was then repeated for each of the three diffraction rings produced by BCC iron.

Results

The strain tensor data for each ring at each load level was tabulated (see Table 4,5,6) and for each ring the calculated strain tensor in the ε_{22} direction (the load axis of the dog bone sample which will demonstrate the most dramatic stain) was plotted in Origin against the stress at each load level as demonstrated in Figure 4. Assuming the elastic deformation is linear with stress and strain, a linear fit of the strain data was taken for each ring. The slope of this fit provided the elastic modulus along each crystallographic direction.

The theoretical values for the elastic modulus along each of the crystallographic planes of the BCC iron were calculated using:

$$\frac{1}{E} = s_{11} - 2[(s_{11} - s_{12}) - \tfrac{1}{2}s_{44}](l_1^2 l_2^2 + l_2^2 l_3^2 + l_1^2 l_{31}^2) \quad (4)$$

Where l_1, l_2, l_3 are the direction cosines for the particular lattice plane as given in Table 1, and the s values are the stiffness constants specific to a given material, shown in Table 2 for iron.

These values are compared to the single crystal values for the elastic modulus in the chosen crystallographic directions in Table 3.

Discussion

The tabulated values for the strain tensor data demonstrate what is expected in terms of sample deformation along particular axes. As the strain increases in the ε_{22} direction, the

strain values in the ε_{33} become negative as would be expected from a material elongating in one direction while contracting in the other direction.

The data as plotted in the ε_{22} graph produces a pretty good linear fit, providing credible elastic modulus values along the different crystallographic directions. The error bars on the individual points, while present, are too small to be noticeable demonstrating a high confidence in the method developed for obtaining strain from 2D diffraction pattern. However, the plotted ε_{22} data sets and fitted lines do not have intercepts at zero because their location on the y-axis depends on the particular unstrained lattice spacing (d0). The data was manually shifted closer to the origin to compensate for the inaccurate estimation of d0 values. Ideally the actual d0 value could be determined by analyzing calibration parameters. In any case, the shifted data does not impact the calculation of the elastic modulus for the different lattice directions.

The measured values for the elastic modulus along the three crystallographic directions are surprisingly dissimilar from each other, and similar to the single crystal values. In fact, the measured value for the (211) plane is exceptionally close to the single crystal value. Rather than exhibiting the behavior expected by continuum mechanics—including the averaging out of strain values as the material was stretched—such a correlation indicates that in the polycrystalline sample used the strain is distributed along the different crystallographic directions in highly anisotropic manner. Thus, although the sample is polycrystalline, the high anisotropy of the crystallographic orientations of iron has a large effect as the sample reacts to stress.

Such a conclusion is problematic because this high anisotropy would seem to indicate that the crystalline structure would deform differently in the same direction depending on

crystallographic orientation resulting in discontinuities between grains in the material, if they are not accommodated by a secondary mode of strain distribution. But the loading procedure utilized is supposed to result in purely elastic – single mode deformation. Certainly continuum mechanics is proven on a larger scale, and the degree of anisotropy demonstrated indicates that more research must be done to determine by what mechanism crystalline structures distribute strain to accommodate the anisotropy observed here while still demonstrating elasticity.

Acknowledgements

This project was performed at the Stanford Linear Accelerator Center in Palo Alto, California. I would like to thank the U.S. Department of Energy for providing the funding and facilities for the Summer Undergraduate Laboratory Internship (SULI) program in which I was allowed to participate. I would also like to thank my mentor, Apurva Mehta, for his guidance, support, and expertise as well as David Bronfenbrenner who worked with me throughout this project.

References

[1] I.C. Noyan, J.B Cohen. *Residual Stress: Measurement by Diffraction and Interpretation.* New York: Springer-Verlag, 1987, pp. 117-120

[2] B.E. Warren. *X-Ray Diffraction*. New York: Dover Publications, 1969, pp. 102-115

[3] Viktor Hauk. *Structural and Residual Stress Analysis by Nondestructive Methods*. New York: Elsevier, 1997. pp. 135-150

[4] Richard W. Hertzberg. *Deformation and Fracture Mechanics of Engineering Materials.* New York: Wiley, 1995. pp.10-16.

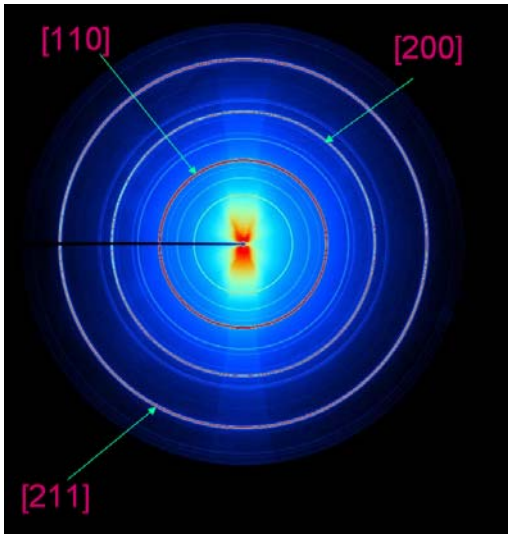

Figure 1. Diffraction pattern for BCC iron highlighting the three analyzed rings.

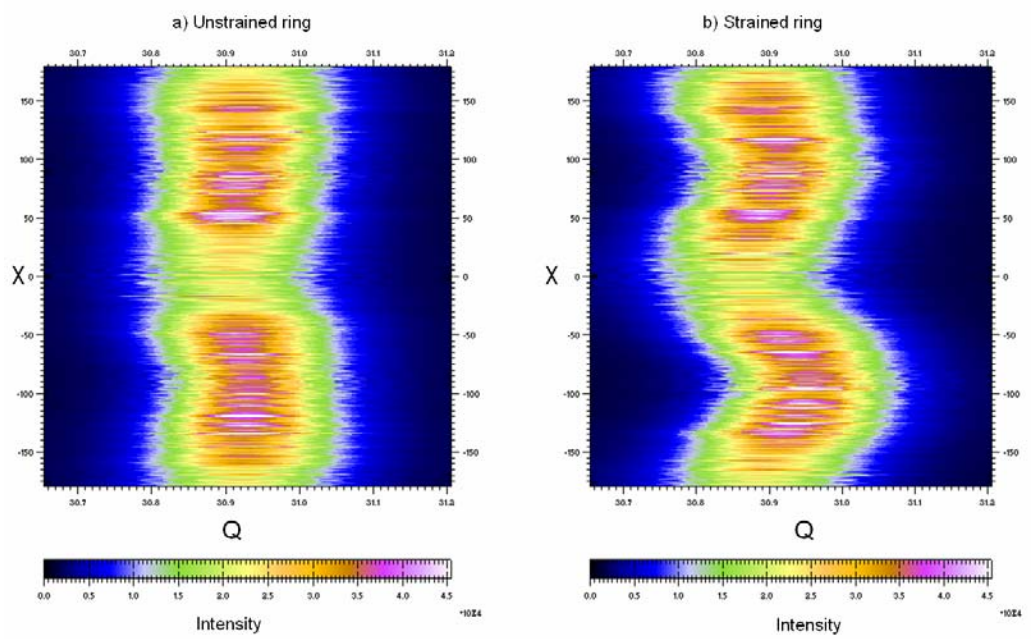

Figure 2. Results of Fit2D coordinate transformation of diffraction pattern to Q/chi space. a) the transformed pattern of an unstrained sample b) the pattern from a strained sample

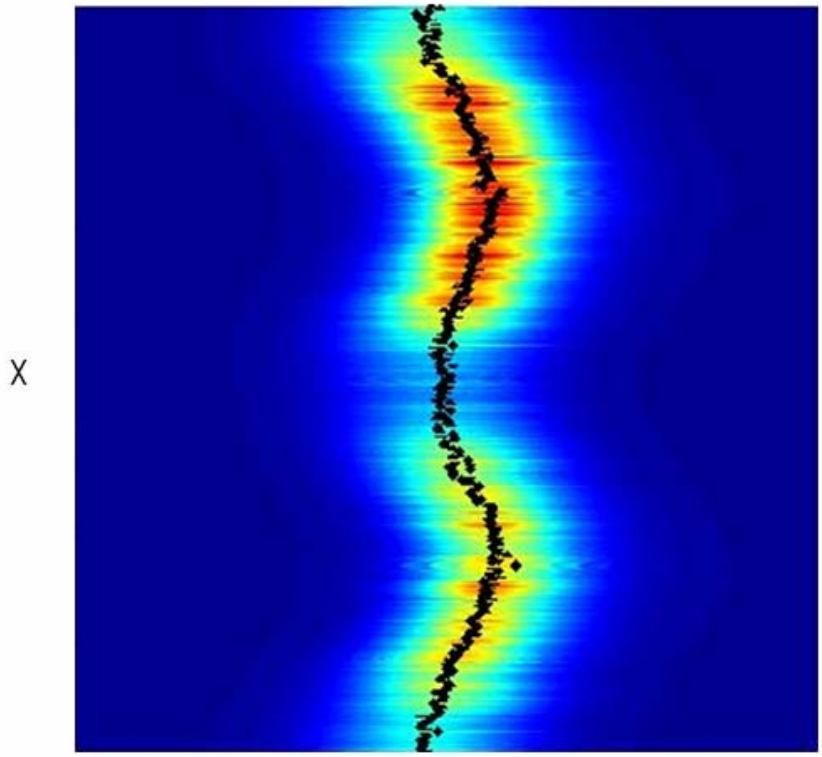

Figure 3. Plot of high intensity points as determined by Gaussian fit for each chi value

Direction	l_1	l_2	l_3
[200]	1	0	0
[110]	$1/\sqrt{2}$	$1/\sqrt{2}$	0
[211]	$2/\sqrt{6}$	$1/\sqrt{6}$	$1/\sqrt{6}$

Table 1. Direction Cosines

a) Established Values

	Elastic Modulus (GPa)
110	210
200	125
211	210

b) Measured Values

	Elastic Modulus (GPa)
110	177 ±11
200	152 ±6
211	207 ±9

Table 3. Established values for Elastic Modulus of single crystal iron

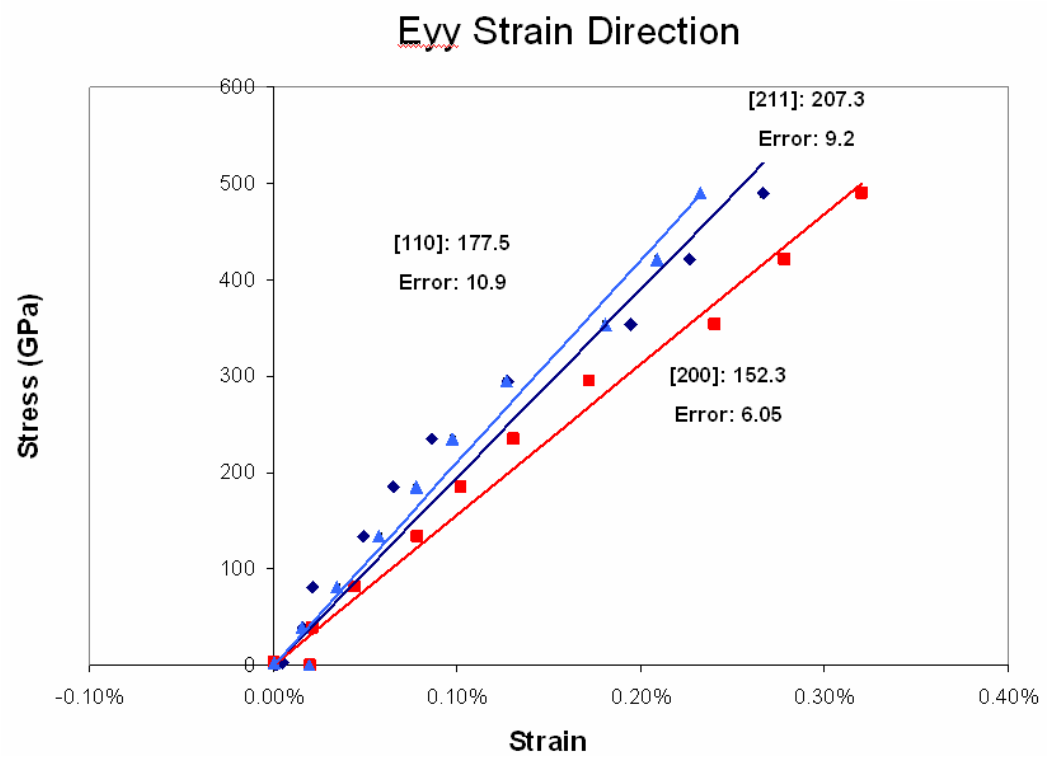

Figure 4. Stress-strain plot for each crystallographic plane along the principle loading direction.

	Load Level (GPa)										
[110]	490.37	420.74	353.33	295.56	234.81	184.44	134.07	80.74	39.26	2.22	0.00
exx	-1.18E-04	2.05E-05	3.04E-05	-4.26E-04	-5.77E-04	-5.32E-04	-7.20E-04	-3.95E-04	-3.62E-05	-2.70E-04	2.32E-04
exx error	4.80E-05	4.92E-05	5.55E-05	7.67E-05	5.54E-05	5.29E-05	6.04E-05	5.24E-05	3.70E-05	3.85E-05	2.67E-05
exy	-8.45E-05	-2.97E-05	-2.01E-05	1.69E-05	-1.58E-04	-2.54E-05	7.13E-05	-2.00E-05	9.06E-05	4.88E-05	4.34E-05
exy error	1.30E-05	1.34E-05	1.51E-05	1.73E-05	1.51E-05	1.44E-05	1.64E-05	1.43E-05	1.00E-05	1.04E-05	7.22E-06
exz	-3.31E-04	-8.40E-05	-9.45E-05	-2.20E-04	6.48E-06	-5.76E-05	-1.74E-04	-1.59E-05	-2.37E-04	-3.45E-04	4.21E-05
exz error	1.97E-05	2.01E-05	2.27E-05	2.32E-05	2.27E-05	2.17E-05	2.47E-05	2.15E-05	1.52E-05	1.58E-05	1.10E-05
eyy	2.67E-03	2.26E-03	1.94E-03	1.27E-03	8.62E-04	6.54E-04	4.85E-04	2.13E-04	1.61E-04	4.93E-05	1.71E-05
eyy error	9.15E-06	9.43E-06	1.06E-05	1.23E-05	1.07E-05	1.02E-05	1.16E-05	1.01E-05	7.08E-06	7.37E-06	5.10E-06
eyz	3.24E-06	2.52E-06	-6.48E-07	4.88E-06	-3.19E-05	-1.09E-05	9.19E-06	-1.48E-05	1.10E-06	1.48E-05	-3.35E-05
eyz error	7.73E-06	7.95E-06	8.96E-06	9.44E-06	8.98E-06	8.57E-06	9.75E-06	8.49E-06	5.97E-06	6.21E-06	4.31E-06
ezz	-4.14E-04	-4.79E-04	-3.95E-04	-7.17E-04	-6.72E-04	-5.99E-04	-4.74E-04	-3.70E-04	-2.99E-04	-1.78E-04	-5.91E-05
ezz error	1.01E-05	1.03E-05	1.17E-05	1.23E-05	1.16E-05	1.11E-05	1.27E-05	1.10E-05	7.78E-06	8.09E-06	5.61E-06

Table 4. Calculated strain tensors for the [110] crystallographic plane

	Load Level (GPa)										
[200]	490.37	420.74	353.33	295.56	234.81	184.44	134.07	80.74	39.26	2.22	0.00
exx	0.003015	0.003054	0.003064	0.002529	0.002578	0.002708	0.002544	0.002703	0.002788	0.00263	0.003075
exx error	4.61E-05	5.52E-05	5.45E-05	8.73E-05	5.41E-05	5.19E-05	5.22E-05	5.05E-05	5.05E-05	5.07E-05	2.24E-05
exy	-2.39E-05	-2.24E-05	-2.32E-05	6.59E-06	-9.68E-05	-2.18E-05	3.49E-05	-2.56E-05	3.64E-05	3.06E-05	7.10E-05
exy error	1.33E-05	1.20E-05	1.19E-05	1.34E-05	1.19E-05	1.14E-05	1.14E-05	1.11E-05	1.10E-05	1.11E-05	6.51E-06
exz	-2.77E-04	4.09E-06	-3.60E-05	-8.97E-05	-5.15E-06	-9.56E-06	-9.18E-05	-1.82E-06	-2.78E-05	-8.72E-05	9.73E-05
exz error	2.05E-05	1.86E-05	1.83E-05	2.01E-05	1.82E-05	1.75E-05	1.75E-05	1.70E-05	1.70E-05	1.70E-05	9.97E-06
eyy	6.05E-03	5.63E-03	5.25E-03	4.56E-03	4.15E-03	3.86E-03	3.63E-03	3.29E-03	3.06E-03	2.85E-03	3.05E-03
eyy error	1.34E-05	1.30E-05	1.28E-05	1.66E-05	1.28E-05	1.23E-05	1.23E-05	1.20E-05	1.19E-05	1.20E-05	6.54E-06
eyz	2.50E-05	1.74E-05	1.50E-05	8.12E-06	-1.68E-05	-8.79E-06	-9.11E-06	-2.23E-05	-1.28E-05	-1.10E-05	-3.98E-05
eyz error	1.00E-05	8.83E-06	8.72E-06	9.64E-06	8.69E-06	8.33E-06	8.35E-06	8.10E-06	8.08E-06	8.13E-06	4.93E-06
ezz	2.49E-03	2.51E-03	2.67E-03	2.46E-03	2.55E-03	2.67E-03	2.83E-03	2.95E-03	3.05E-03	3.13E-03	3.10E-03
ezz error	1.33E-05	1.22E-05	1.20E-05	1.55E-05	1.20E-05	1.15E-05	1.15E-05	1.12E-05	1.11E-05	1.12E-05	6.45E-06

Table 5. Calculated strain tensors for the [200] crystallographic plane

	Load Level (GPa)										
	490.37	420.74	353.33	295.56	234.81	184.44	134.07	80.74	39.26	2.22	0.00
exx	1.37E-03	9.70E-04	9.75E-04	6.98E-04	6.36E-04	7.36E-04	7.84E-04	7.32E-04	7.48E-04	6.51E-04	8.11E-04
exx error	4.04E-05	2.76E-05	2.56E-05	3.03E-05	2.22E-05	2.36E-05	2.45E-05	2.41E-05	1.89E-05	2.06E-05	1.25E-05
exy	3.39E-05	-8.06E-06	-5.91E-06	1.09E-05	-4.34E-05	2.87E-07	3.96E-05	-6.03E-07	3.94E-05	3.72E-05	6.85E-05
exy error	9.60E-06	6.56E-06	6.09E-06	5.07E-06	5.28E-06	3.95E-06	4.08E-06	4.03E-06	4.47E-06	4.89E-06	2.95E-06
exz	-2.15E-04	9.99E-07	-1.51E-05	-4.03E-05	5.34E-06	-1.29E-05	-3.97E-05	-9.72E-07	-1.51E-05	-4.40E-05	2.75E-05
exz error	1.46E-05	9.93E-06	9.21E-06	7.48E-06	7.97E-06	5.81E-06	6.03E-06	5.93E-06	6.80E-06	7.43E-06	4.49E-06
eyy	2.32E-03	2.09E-03	1.80E-03	1.27E-03	9.72E-04	7.75E-04	5.75E-04	3.45E-04	1.55E-04	0.00E+00	1.95E-04
eyy error	1.36E-05	9.32E-06	8.64E-06	8.53E-06	7.50E-06	6.65E-06	6.88E-06	6.78E-06	6.37E-06	6.96E-06	4.19E-06
eyz	3.63E-05	1.37E-05	1.26E-05	5.30E-06	-6.92E-06	-4.61E-06	-4.19E-06	-1.09E-05	-1.28E-06	1.63E-06	-2.49E-05
eyz error	8.61E-06	5.88E-06	5.45E-06	4.53E-06	4.72E-06	3.53E-06	3.65E-06	3.60E-06	4.01E-06	4.39E-06	2.64E-06
ezz	2.31E-04	3.30E-04	4.53E-04	2.72E-04	3.38E-04	4.53E-04	5.55E-04	6.42E-04	6.95E-04	7.54E-04	7.00E-04
ezz error	1.24E-05	8.42E-06	7.81E-06	7.87E-06	6.76E-06	6.12E-06	6.33E-06	6.24E-06	5.75E-06	6.29E-06	3.77E-06

Table 6. Calculated strain tensors for the [210] crystallographic plane

Comment [DJB1]: Parenthesis when talking about planes, brackets when talking about direction.